Chinese Chemical Letters 32 (2021) 1131–1134

Contents lists available at ScienceDirect

Chinese Chemical Letters

journal homepage: www.elsevier.com/locate/cclet

Communication

Size-controlled flow synthesis of metal-organic frameworks crystals monitored by *in-situ* ultraviolet–visible absorption spectroscopy

Wenbo Li[a,b,e], Yucen Li[c], Wei Zhang[c], Difeng Yin[a,b,e], Ya Cheng[a,c,d,e], Wei Chu[d,*], Ming Hu[c,*]

[a] State Key Laboratory of High Field Laser Physics and CAS Center for Excellence in Ultra-Intense Laser Science, Shanghai Institute of Optics and Fine Mechanics (SIOM), Chinese Academy of Sciences (CAS), Shanghai 201800, China
[b] School of Physical Science and Technology, ShanghaiTech University, Shanghai 200031, China
[c] State Key Laboratory of Precision Spectroscopy, School of Physics and Electronic Science, East China Normal University, Shanghai 200241, China
[d] XXL – The Extreme Optoelectromechanics Laboratory, School of Physics and Electronic Science, East China Normal University, Shanghai 200241, China
[e] University of Chinese Academy of Sciences, Beijing 100049, China

ARTICLE INFO

Article history:
Received 27 August 2020
Received in revised form 18 September 2020
Accepted 23 September 2020
Available online 24 September 2020

Keywords:
Nanoporous particles
Microfluidics
Flow synthesis
Metal-organic frameworks
UV–vis absorption spectrum
Femtosecond laser micromachining

ABSTRACT

Size-controlled flow synthesis of nanoporous particles are of considerable interest for future industrial applications, however, is facing challenges due to lack of *in-situ* method for size-characterization in fluidic environment. We present that ultraviolet-visible (UV–vis) absorption spectroscopy can be integrated into a flow-synthesis system which was produced by femtosecond laser micromachining. The shift of the absorption peak position of the *ex-situ* and *in-situ* UV–vis spectra correlates to variation of size of porous metal-organic frameworks crystals. ZIF-67 crystals with a size in the range from 200 nm to 1025 nm are fabricated with the assistance of tri-ethylamine under monitoring of *in-situ* UV–vis spectra. The ZIF-67 crystals are converted into nanoporous carbons particles with controlled sizes. These materials show size-dependent performance in Na-ion battery and size-independent performance in metal/H_2O seawater battery.

Nanoporous particles, including crystalline and non-crystalline forms, are widely used in applications such as catalysis, separation, and energy storage, *etc.* [1–6]. Particle size is an important parameter in determining performance of the nanoporous particles in applications where diffusion kinetics of guests and specific surface areas play vital roles [7,8]. To liberate labor cost in size-controlled synthesis of nanoporous particles, it is highly needed to develop autonomous procedures. Continuous flow synthesis is a promising synthetic strategy which is suitable for autonomous operations [9–11]. However, one obstacle for establishing an autonomous flow synthesis is that there lack of an *in-situ* method to monitor the size of nanoporous particles during synthetic procedure [12,13]. Electron microscopy is commonly used for characterization of sizes of particles. But this method basically requires the dried particles rather than the particles dispersed in solvents. UV–vis spectroscopy is suitable for measuring the particles dispersed in solvents. Once we can establish relationship between the ultraviolet–visible spectrum and the sizes of nanoporous particles, an autonomous flow synthesis of nanoporous particles will be possible in the future.

Here we present an UV–vis spectroscopy monitored size-controlled flow synthesis of nanoporous particles. The target materials are porous crystalline metal-organic frameworks (MOFs) and their thermo-derivatives. The MOFs and their thermo-derivatives show great promise in wide applications such as energy storage and conversion, catalysis, adsorption and separation [14–26]. Significant size-dependent performance has been observed during utilization of these materials [27,28]. So far, size-controlled flow syntheses of MOFs under in-line monitoring remains a challenge. We designed and fabricated a continuous flow microfluidic chip using femtosecond laser micromachining [29–31], and set up flow synthetic instruments to collect *in-situ* UV–vis spectrum of the generated MOFs particles (Figs. 1, 2 and Fig. S1 in Supporting information). The shift of characteristic peaks in the UV–vis spectrum helps us to determine the size of the particles during synthesis. The size of the nanoporous particles are well-controlled, leading to good performance in sodium ion battery and seawater battery.

* Corresponding authors.
E-mail addresses: wchu@phy.ecnu.edu.cn (W. Chu), mhu@phy.ecnu.edu.cn (M. Hu).

https://doi.org/10.1016/j.cclet.2020.09.039
1001-8417/

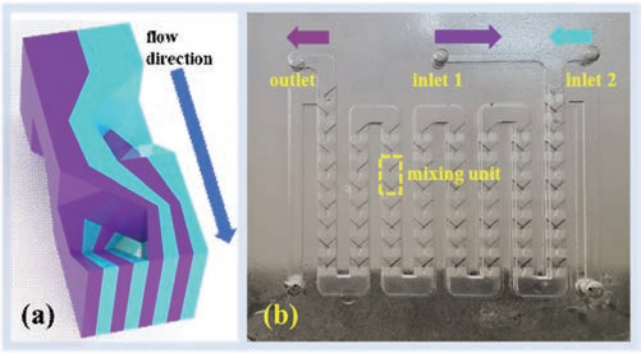

Fig. 1. (a) Schematic view of working mechanism of microfluidic chip. The two microfluidic streams can be divided into eight sub-streams in a mixing unit. (b) Photograph of the fabricated microfluidic chip captured by a camera.

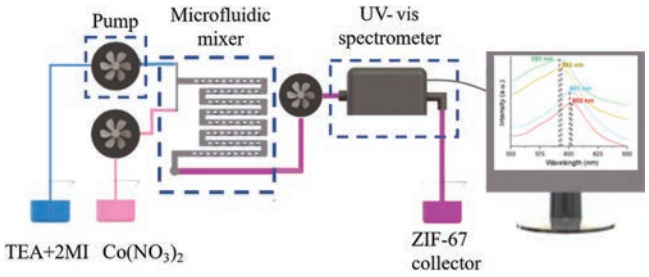

Fig. 2. Schematic illustration of flow synthesis system. TEA represents tri-ethylamine. 2MI represents 2-methylimidazole. In brief, the reactants are pumped into the microfluidic mixer and coordinated inside the mixer. The produced crystals flow with the solvent and are pumped into the UV–vis spectrometer for in-line absorption test. The peak position of the absorption spectrum varies according to the size of the crystals. Therefore, the size of the crystals can be read out automatically.

To facilitate *in-situ* size monitoring, we investigate correlation between the size of ZIF-67 particles and *ex-situ* UV–vis spectra of their methanol dispersion. Fig. S2 (Supporting information) shows SEM image of the prepared ZIF-67 particles. Almost all the samples show a rhombic dodecahedron shape. The size of the particles was controlled by addition of triethylamine according to previous report [32]. Basically, triethylamine can enhance de-protonation of 2-methylimidazole by reacting with protons. The de-protonated 2-methylimidazole can easily coordinate with Co^{2+} ions, forming frameworks fast. In general, fast crystallization leads to smaller particle sizes. With increase of dosage of the triethylamine from 0 to 1.2 mL, the crystal size was reduced from 1208 ± 500 nm to 180 ± 60 nm. We dispersed these particles into methanol solution, and recorded their UV–vis spectra. An absorption peak around 600 nm is observed in all the spectra (Fig. S3 in Supporting information). This peak belongs to the higher-lying $[^4A_2(F) - {}^4T_1(P)]$ d−d ligand field transition for Co^{2+} ion in T_d environment in ZIF-67 [33–35]. For comparison, we measured UV–vis spectrum of triethylamine and methanol solution (Fig. S4 in Supporting information). No absorption peak can be found in this spectrum, confirming that the characteristic peak belongs to ZIF-67. Blue shift (hypsochromic shift) of this peak happens with size-reduction of the ZIF-67 particles. The center of the absorption peak was changed from 604 nm to 590 nm with decrease of the particle size. To explore whether the blue-shift is caused by interaction with the polar solvent, methanol, we changed the dispersion solvent of the ZIF-67 particles from methanol to a solvent with lower polarity, ethanol and acetonitrile. Fig. S5 (Supporting information) illustrates that the blue shift value was reduced to 12 nm in ethanol and 10 nm in acetonitrile when the ZIF-67 crystals with sizes around

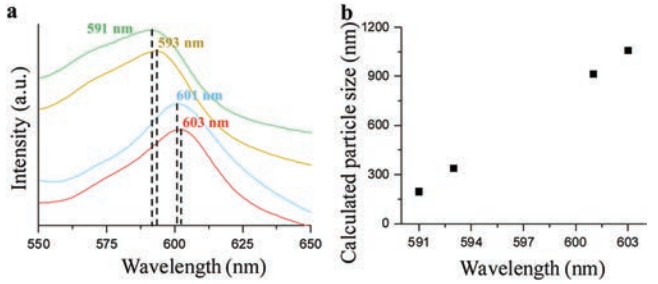

Fig. 3. (a) *In-situ* UV–vis spectra of ZIF-67 particles synthesized by flow synthesis method. (b) Calculated particle size based on position of UV–vis absorption spectra.

∼1208 and ∼180 nm were compared. This result suggests that the larger blue shift (14 nm) in the methanol is probably due to the increased interaction between the methanol solvent and the ZIF-67 particles of the surface areas by reducing the size of the ZIF-67 particles. We plot the absorption peak position *versus* statistic size of the particles in Fig. S6 (Supporting information). Linear relationship is given by

$$S = 0.01395\ W + 588.26172 \quad (1)$$

where S is the size of the particle, and W is the wavelength of the characteristic absorption peak. The relationship means that we may use the blue-shift of the peak near 600 nm to probe the sizes of the ZIF-67 particles during flow synthesis.

We establish a flow synthesis system as shown in Fig. 2. Typically, size-adjusting reagent, tri-ethylamine, was mixed with a methanol solution of 2-methylimidazole. Then, the mixed solution was pumped to react with $Co(NO_3)_2{\cdot}6H_2O$ which is dissolved in methanol solution. The purple solution was guided through an UV–vis spectrometer for *in-situ* characterization, then collected in a product container for further washing. Fig. 3a illustrates *in-situ* UV–vis spectra of the samples which are prepared with varied triethylamine amount. These *in-situ* spectra are of similar shape and peak position as the *ex-situ* spectra. A characteristic peak centered at near 600 nm exist in all the spectra. Shift of the peak position is observed. On the basis of the position of the absorption peak, the sizes of the obtained crystals are estimated by Eq. 1 and listed in Fig. 3b. To exemplify validity of our estimation, we used SEM to characterize the shape and size of the product. The products are of typical shape of ZIF-67 as shown in Fig. S7 (Supporting information). Statistic size of the ZIF-67 crystals were collected by measuring rhombic dodecahedron particles in each SEM image. We compared the SEM-measured sizes and the estimated sizes based on the *in-situ* UV–vis spectra as shown in Fig. 4. A good matching exists between the two set of data, indicating that the *in-situ* UV–vis spectra can be used to estimate the sizes of the final products. We note that the size of the crystals correlates to the dosage amount of the tri-ethylamine during the

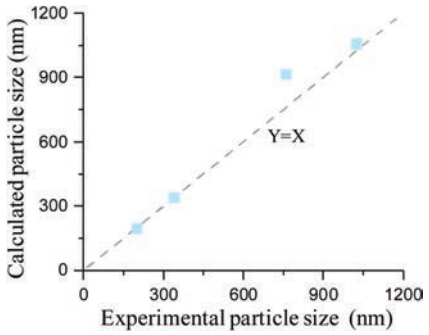

Fig. 4. Comparison of the calculated and experimental sizes of the ZIF-67 particles synthesized by flow synthesis method.

flow synthesis. This is similar to the phenomena happened in bulk synthesis, indicating that the tri-ethylamine is effective in a flow synthetic environment.

Powder XRD profiles of the samples match with the simulated pattern from the single-crystal diffraction data of ZIF-67, indicating successful synthesis of sodalite ZIF-67 (Fig. S8a in Supporting information). No other peaks are found, suggesting the high purity of our products. These ZIF-67 particles are highly porous due to their high crystallinity. Fig. S8b (Supporting information) illustrates N_2 sorption isotherms of these products at 77 K. All the samples present type I adsorption behavior, confirming their microporous nature. All the samples have similar specific surface areas according to Brunauer-Emmett-Teller (BET) method. The largest crystals (~1025 nm) have a BET surface area of about 1396 m^2/g, while the smallest crystals show a BET surface area near 1347 m^2/g.

These ZIF-67 particles can be derived into nanoporous carbons, which is a suitable strategy in producing hybrid nanoporous carbons with good charge or ions adsorption/intercalation capability and high catalytic activity. In order to obtain the nanoporous carbon with controlled sizes, the as synthesized ZIF-67 samples were directly carbonized at 600 °C under the protection of N_2 atmosphere. The obtained products were characterized by SEM, powder XRD and N_2 sorption analysis. Fig. S9a (Supporting information) illustrates that the nanoporous carbons (ZIF-67-C) maintain the shape and size of initial ZIF-67 samples basically. However, the faces of the acquired carbons shrink at different degree during carbonization. The shrinkage degree is consistent with size of the particles. The smallest ZIF-67-C particles heavily shrunk, and their initial rhombic faces got vanished completely. In contrast, the largest ZIF-67 particles yield the carbons with similar rhombic dodecahedron as the initial ZIF-67 crystals. Powder XRD profiles of these carbons show three diffraction peaks at near 26°, 44° and 51°, which can be is indexed as (002) plane of graphite, (111) and (200) planes of Co, respectively (Fig. S9b in Supporting information). The residual metallic Co was formed by reduction of the divalent cobalt ions during pyrolysis. The nitrogen adsorption-desorption isotherms of the obtained carbons are shown in Fig. S9c (Supporting information). Hysteresis loops are in the isotherms of all the samples, indicating high porosity of all the carbons. The BET specific surface areas of the samples are quite similar, from 440 m^2/g to 450 m^2/g. This result matches with the pore-size distribution data of the samples (Fig. S10 in Supporting information). All the samples are of microporous structures rather than mesoporous structures.

Because of the existence of nitrogen atoms in the 2-methylimidazole ligands, the obtained nanoporous carbons are doped by nitrogen atoms which can optimize electrochemical properties of the carbons. Fig. S11 (Supporting information) illustrates XPS spectra of the samples. All the ZIF-67-derived samples are mainly composed of C, N, O and Co elements. The analytical results are summarized and listed in Table S1 (Supporting information). The results indicate the three samples have quite similar compositions. In the C 1s spectra, two main peaks at around 284.6± 0.2 eV and 285.1 ± 0.1 eV correspond to sp^2 and sp^3 hybridization of carbon. The nitrogen atoms have been successfully doped into the samples as confirmed by the existence of C-N peak (285.9 ± 0.2 eV). In addition, the other peaks at 286.8 ± 0.2 eV and 288.6 ± 0.2 eV are ascribed to C=O and COOR [36,37]. The Co element, as the main composition of ZIF-67, also show strong peaks in XPS spectra. The main peak at 778.0 ± 0.2 eV in the Co 2p spectra are attributed to zero-valent Co, which suggests that Co^{II} ions in ZIF-67 are reduced to metallic state. The other peaks locating at 779.0 ± 0.2 eV, 780.4 ± 0.2 eV and 781.8 ± 0.2 eV are attributed to Co_xO_y or CoC_xN_y, Co_xO_y, CoN_x, respectively [38,39]. As for the N 1s spectra, all the samples are composed of pyridinic-N (398.6 ± 0.1 eV), pyrrolic-N (399.6 ± 0.2 eV), and graphitic-N (400.8 ± 0. 2 eV), which matches well with C 1s spectra [40].

The nanoporous carbon particles doped by nitrogen atoms are promising electrode materials for sodium ion battery. To investigate their electrochemical property, cyclic voltammetry (CV) and galvanostatic discharge/charge test were applied in a C/Na half-cell configuration (Fig. S12 in Supporting information). In the CV profiles, a broad peak at around 0.5 V and a sharp peak near 0 V in the reduction curve can be assigned to insertion of the sodium ions to graphene layers and nanopores respectively. The oxidation curve almost overlaps the curve of the initial cycle. Fig. S12d shows the galvanostatic profiles of the samples in a range of 0~3 V at a current rate of 50 mA/g. The smallest sample (ZIF-67-C (340)) has a discharge capacity of 276 mAh/g, and a charge capacity of 250 mAh/g. Both capacities are higher than that of the larger sample (ZIF-67-C (1025)). Fig. S13a (Supporting information) shows rate performance of the nanoprorous carbons. The ZIF-67-C (340) sample exhibits the best rate performance compared to other two electrodes. The results illustrate that the particle size play a vital role in storage of sodium ions. The diffusion distance of sodium ions in each sample may be the influence factor caused by particle size. The large sample has long diffusion distance which may prevent diffusion of the sodium ion from reaching the inner part of a porous particle, especially when the current density is high. Therefore, the largest sample is not good for high rate sodium ions storage. The cycling performance of the samples is shown in Fig. S13b (Supporting information). The electrode made by ZIF-67-C (340) also displays the most remarkable stability. The reversible capacity was maintained at as high as 212 mAh/g after 200 cycles at a current density of 50 mA/g, while the capacity of other two samples were 178 and 163 mAh/g respectively. The ZIF-67-C (340) with small size and porous structure could facilitate the migration of sodium ion and contact area between electrolyte and electrode which as a promising material for practical application of SIBs in future.

The nanoporous carbons can also be used as catalyst for hydrogen evolution which is a vital step for Mg/H_2O seawater battery. This kind of battery generates electric current through electron transfer from the Mg electrode to H_2O molecules, thus has ultra long working life and high energy density but requires usage of precious catalysts [41–43]. The nanoporous carbons prepared in this work are expected to be a potential replacement of the Pt catalyst used in the current Mg/H_2O seawater battery. We fabricated a Mg/H_2O seawater battery by using the nanoporous carbons as the catalyst in a cathode, a piece of Mg plate as the anode, and filtered seawater taken from the Donghai sea (Shanghai, China) as the electrolyte (Fig. S14a in Supporting information). For comparison, the nanoporous carbons with two average sizes were used. The polarization curves and the corresponding power density plots of the Mg/H_2O battery assembled with both samples are shown in Fig. S14b (Supporting information). For the ZIF-67-C (340) sample, the output power densities are 0.52, 1.75, 2.42, 1.96 and 0.06 mW/cm^2 at current densities of 1, 5, 10, 20 and 30 mA/cm^2, respectively. For the ZIF-67-C (1025) sample, the output power densities are 0.51, 1.65, 2.22, 2.2 and 1.21 mW/cm^2 at current densities of 1, 5, 10, 20 and 30 mA/cm^2, respectively. Both samples show similar performance on Mg/H_2O seawater battery at various current rates. The stability of both samples was tested also. The corresponding seawater batteries were evaluated by galvanostatic discharging at 5 mA/cm^2 for 50 h as displayed in Fig. S14c (Supporting information). The output voltage of both batteries is around 0.35 V, almost without any fluctuation in whole day. This result indicates that the ZIF-67-derived nanoporous carbon is an ultra-stable catalyst for water-splitting. In addition, we compared the power density and theoretical energy density of our system to other reported systems

(Table S2 in Supporting information) [41–43]. Indeed, our system has comparable performance. For applying our system into practical use, we used the fabricated Mg/H_2O battery to light up a red light-emitting diode as shown in Fig. S14d (supporting information).

In summary, we demonstrated that UV–vis absorption spectroscopy could be integrated into a flow-synthesis system. The absorption peak position of the UV–vis absorption spectra linearly related to the size of ZIF-67 crystals, therefore an inline UV–vis absorption spectroscopy method became possible. The crystals with controlled sizes in the range from 200 nm to 1025 nm were synthesized through flow chemisty under inline monitoring of the UV–vis absorption spectra. The ZIF-67 crystals were converted into nanoporous carbons particles, and showed size-dependent performance in Na-ion battery and size-independent performance in Mg/H_2O seawater battery.

Declaration of competing interest

The authors report no declarations of interest.

Acknowledgments

The work is supported by National Natural Science Foundation of China (Nos. 11674340, 21473059); Key Project of the Shanghai Science and Technology Committee (No. 18DZ1112700).

Appendix A. Supplementary data

Supplementary material related to this article can be found, in the online version, at doi:https://doi.org/10.1016/j.cclet.2020.09.039.

References

[1] A. Glotov, A. Stavitskaya, Y. Chudakov, et al., Bull. Chem. Soc. Jpn. 92 (2019) 61–69.
[2] N.L. Torad, M. Hu, S. Ishihara, et al., Small 10 (2014) 2096–2107.
[3] I.I. Slowing, J.L. Vivero-Escoto, C.W. Wu, V.S.Y. Lin, Adv. Drug Deliv. Rev. 60 (2008) 1278–1288.
[4] H. Tan, J. Tang, J. Kim, et al., J. Mater. Chem. A 7 (2019) 1380–1393.
[5] K. Ariga, A. Vinu, Y. Yamauchi, Q.M. Ji, J.P. Hill, Bull. Chem. Soc. Jpn. 85 (2012) 1–32.
[6] V. Malgras, Q.M. Ji, Y. Kamachi, et al., Bull. Chem. Soc. Jpn. 88 (2015) 1171–1200.
[7] H. Ming, N.L.K. Torad, Y.D. Chiang, K.C.W. Wu, Y. Yamauchi, CrystEngComm 14 (2012) 3387–3396.
[8] N.L. Torad, M. Hu, Y. Kamachi, et al., Chem. Commun. 49 (2013) 2521–2523.
[9] A.C. Bedard, A. Adamo, K.C. Aroh, et al., Science 361 (2018) 1220.
[10] S. Chatterjee, M. Guidi, P.H. Seeberger, K. Gilmore, Nature 579 (2020) 379.
[11] D.J. Walsh, D.A. Schinski, R.A. Schneider, D. Guironnet, Nat. Commun. 11 (2020) 9.
[12] M. Rubio-Martinez, C. Avci-Camur, A.W. Thornton, et al., Chem. Soc. Rev. 46 (2017) 3453–3480.
[13] C. Hu, Y.X. Bai, M. Hou, et al., Sci. Adv. 6 (2020) 8.
[14] W. Xia, A. Mahmood, R.Q. Zou, Q. Xu, Energy Environ. Sci. 8 (2015) 1837–1866.
[15] A. Azhar, Y. Li, Z. Cai, et al., Bull. Chem. Soc. Jpn. 92 (2019) 875–904.
[16] L. Wang, Y.Z. Han, X. Feng, et al., Coord. Chem. Rev. 307 (2016) 361–381.
[17] J.D. Xiao, H.L. Jiang, Acc. Chem. Res. 52 (2019) 356–366.
[18] Q. Gao, J. Xu, X.H. Bu, Coord. Chem. Rev. 378 (2019) 17–31.
[19] Y.X. Chen, W. Zhang, X.F. Jiang, et al., Mater. Chem. Front. 2 (2018) 520–529.
[20] Y.Y. Zhao, X. Li, M. Hu, Chin. Chem. Lett. 30 (2019) 630–633.
[21] C.F. Wang, W. Zhang, W.W. Li, et al., Chin. Chem. Lett. 30 (2019) 1390–1392.
[22] Y.T. Liao, N.V. Chia, N. Ishiguro, et al., Appl. Catal. B 270 (2020) 118805.
[23] Y.T. Liao, B.M. Matsagar, K.C.W. Wu, ACS Sustainable Chem. Eng. 6 (2018) 13628–13643.
[24] H. Konnerth, B.M. Matsagar, S. S.Chen, et al., Coord. Chem. Rev. 416 (2020) 213319.
[25] C.C. Chueh, C.I. Chen, Y.A. Su, et al., J. Mater. Chem. A 7 (2019) 17079–17095.
[26] C.C. Lee, C.I. Chen, Y.T. Liao, K.C.W. Wu, C.C. Chueh, Adv. Sci. 6 (2019) 1801715.
[27] J. Park, Q. Jiang, D.W. Feng, L.Q. Mao, H.C. Zhou, J. Am. Chem. Soc. 138 (2016) 3518–3525.
[28] A. Tiba, A.V. Tivanski, L.R. MacGillivray, Nano Lett. 19 (2019) 6140–6143.
[29] P. Carrière, Phys. Fluids 19 (2007) 118110.
[30] K. Sugioka, Y. Cheng, Light Sci. Appl. 3 (2014) e149.
[31] J. Qi, W.B. Li, W. Chu, et al., Micromachines 11 (2020) 213.
[32] W. Zhang, X.F. Jiang, X.B. Wang, et al., Angew. Chem. Int. Ed. 56 (2017) 8435–8440.
[33] B. Pattengale, S.Z. Yang, J. Ludwig, et al., J. Am. Chem. Soc. 138 (2016) 8072–8075.
[34] K.V. Yumashev, I.A. Denisov, N.N. Posnov, N.V. Kuleshov, R. Moncorge, J. Alloys. Compd. 341 (2002) 366–370.
[35] R. Trujillano, F. Villain, C. Louis, J.F. Lambert, J. Phys. Chem. C 111 (2007) 7152–7164.
[36] Z.L. Yu, S. Xin, Y. You, et al., J. Am. Chem. Soc. 138 (2016) 14915–14922.
[37] S.W. Lee, N. Yabuuchi, B.M. Gallant, et al., Nat. Nanotechnol. 5 (2010) 531–537.
[38] Y.Z. Chen, C. Wang, Z.Y. Wu, et al., Adv. Mater. 27 (2015) 5010–5016.
[39] A. Morozan, P. Jegou, B. Jousselme, S. Palacin, Phys. Chem. Chem. Phys. 13 (2011) 21600–21607.
[40] W. Zhang, S. Bu, Q. Yuan, Q. Xu, M. Hu, J, Mater. Chem. A 7 (2019) 647–656.
[41] P.K. Shen, A.C.C. Tseung, C. Kuo, J. Power Sources 47 (1994) 119–127.
[42] Q. Liu, Z. Yan, E. Wang, S. Wang, G. Sun, Int. J. Hydrogen Energy 42 (2017) 23045–23053.
[43] P.K. Shen, A.C.C. Tseung, J. Appl. Electrochem. 24 (1994) 145–148.